JACS Au
AN OPEN ACCESS JOURNAL OF THE AMERICAN CHEMICAL SOCIETY

pubs.acs.org/jacsau
Article

Cucurbit[8]uril Confinement-Based Secondary Coassembly for High-Efficiency Phosphorescence Energy Transfer Behavior

Xian-Yin Dai, Qi Song, Wei-Lei Zhou, and Yu Liu*

Cite This: https://doi.org/10.1021/jacsau.3c00642
Read Online

ACCESS | Metrics & More | Article Recommendations | Supporting Information

ABSTRACT: Aqueous supramolecular long-lived near-infrared (NIR) material is highly attractive but still remains great challenge. Herein, we report cucurbit[8]uril confinement-based secondary coassembly for achieving NIR phosphorescence energy transfer in water, which is fabricated from dicationic dodecyl-chain-bridged 4-(4-bromophenyl)-pyridine derivative (G), cucurbit[8]uril (CB[8]), and polyelectrolyte poly(4-styrene-sulfonic sodium) (PSS) via the hierarchical confinement strategy. As compared to the dumbbell-shaped G, the formation of unprecedented linear polypseudorotaxane G⊂CB[8] with nanofiber morphology engenders an emerging phosphorescent emission at 510 nm due to the macrocyclic confinement effect. Moreover, benefiting from the following secondary assembly confinement, such tight polypseudorotaxane G⊂CB[8] can further assemble with anionic polyelectrolyte PSS to yield uniform spherical nanoparticle, thereby significantly strengthening phosphorescence performance with an extended lifetime (i.e., 2.39 ms, c.f., 45.0 μs). Subsequently, the organic dye Rhodamine 800 serving as energy acceptor can be slightly doped into the polyelectrolyte assembly, which enables the occurrence of efficient phosphorescence energy transfer process with efficiency up to 80.1% at a high donor/acceptor ratio, and concurrently endows the final system with red-shifted and long-lived NIR emission (710 nm). Ultimately, the as-prepared assembly is successfully exploited as versatile imaging agent for NIR window labeling and detecting in living cells.

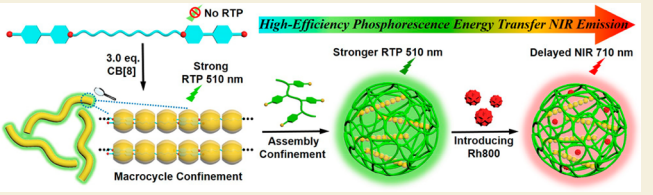

KEYWORDS: *cucurbit[8]uril, phosphorescence, energy transfer, NIR emission, cell imaging*

INTRODUCTION

Supramolecular near-infrared (NIR) emissive materials have aroused significant research interest owing to their outstanding features such as good spatial resolution, deep tissue penetration, and low background noise, which possess promising application values in the fields of biological imaging,[1−4] disease theranostics,[5−7] organic light-emitting devices,[8,9] and biomedical sensors.[10−12] Particularly, macrocycle-involved host−guest complexation have been turned out to be a valid strategy to construct NIR luminescent materials especially in aqueous environment.[13−16] The guest chromophores are tightly encapsulated into the cavity of well-crafted artificial macrocyclic hosts like cyclodextrins,[17,18] cucurbiturils,[19−22] and pillararenes[23,24] enabled by noncovalent interactions, which can alter molecular conformation and packing modes, thereby ultimately restricting molecular rotation or forming J-aggregates with enhanced red-shifted emissions. Alternatively, Föster resonance energy transfer (FRET)-based supramolecular artificial light-harvesting system is recognized as another feasible protocol to realize long-range NIR luminescence with large Stokes shift at a relatively high donor/acceptor ratio,[25−29] which concurrently avoids burdensome covalent chemical synthesis or modification of fluorophores and endows the system with precise controllability. However, the nanosecond-level lifetimes arising from the inherent properties of most existing luminogens have severely obstructed their further practical applications. As a result, the convenient fabrication of NIR emitting material with long lifetime in aqueous media is still a formidable challenge.

To alleviate above issues, purely organic room-temperature phosphorescence (RTP) have drawn into the limelight by virtue of their intrinsic photophysical characteristics including long-lived excited states and large Stokes shifts.[30−34] Recently, supramolecular confinement strategy derived from multiple interactions can not only effectively induce phosphorescent generation and then boost its emission in both the solution and the solid state but also create assembled environment to perform the triplet-involved phosphorescence resonance energy transfer process.[35−39] Thus, the utilization of phosphors as donors stands for a kind of excellent alternatives for constructing afterglow luminescent supramolecular materials, which powerfully allows for the miscellaneous applications in information safety,[40−42] biorelated imaging,[43−46] and color-

Received: October 21, 2023
Revised: November 29, 2023
Accepted: November 30, 2023
Published: December 20, 2023

Scheme 1. Schematic Illustration of the Fabrication of the Multivalent Nanoparticle for High-Efficiency NIR Phosphorescence Resonance Energy Transfer

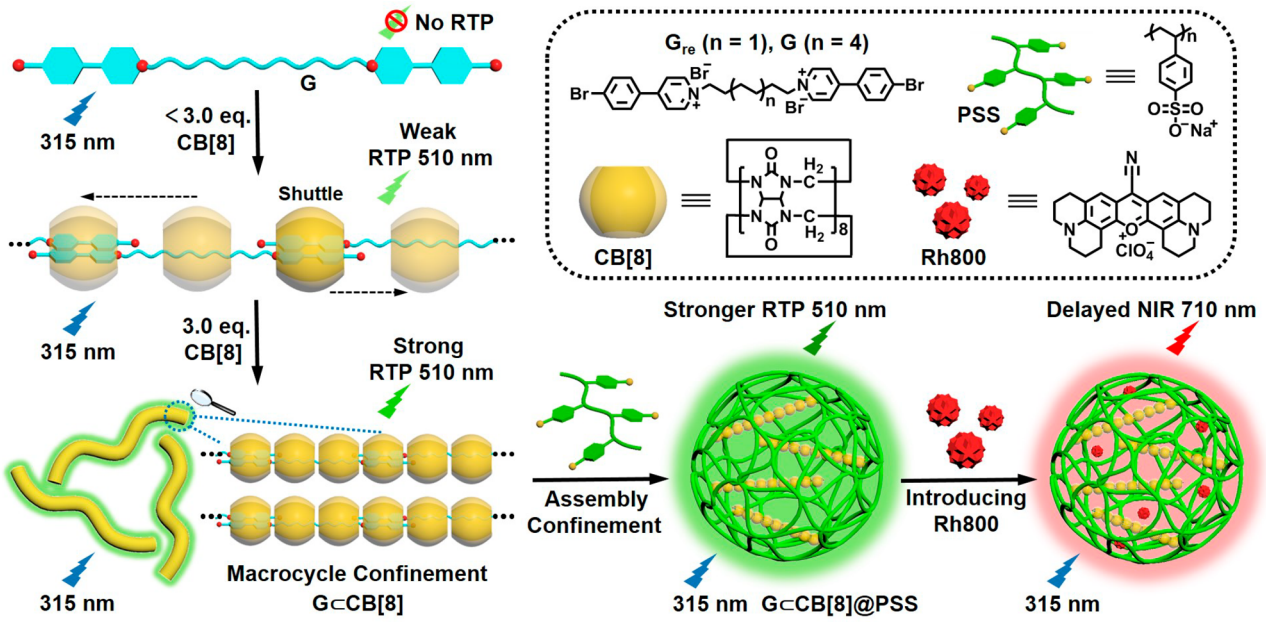

resolved display.[47,48] For example, Chen et al. reported a highly efficient deep-blue phosphorescence by incorporating trimesic acid into self-assembled 2D hydrogen-bonded superlattices, which further realized full-color afterglow displays via energy transfer by introducing different fluorescent dyes.[49] George and co-workers reported an efficient organic−inorganic light-harvesting platform in water which successfully achieved delayed fluorescence through a delayed sensitization process.[50] Despite the ongoing research on fabricating water-soluble supramolecular phosphorescence energy transfer systems, achieving the long-lived NIR-emitting phosphorescence energy transfer system with NIR window cell imaging and sensing capacity has rarely been reported.

Herein, we constructed a highly efficient phosphorescence energy transfer system based on cucurbit[8]uril-confined secondary coassembly via the hierarchical confinement strategy, which was composed of dicationic dodecyl-chain-bridged 4-(4-bromophenyl)-pyridine derivative (G), cucurbit[8]uril (CB[8]), and poly(4-styrene-sulfonic sodium) (PSS), with the aim of attaining long-lived NIR emission in water and exploring its potential applicability for NIR imaging and sensing (Scheme 1). Concretely, the first host−guest confinement enabled that dumbbell-shaped G could be fully encapsulated by CB[8] leading to forming unprecedented linear polypseudorotaxane G⊂CB[8] with nanofiber morphology, concurrently accompanied by the induced phosphorescent emission at 510 nm. Subsequently, the assembly confinement resulting from the multivalent interactions between the noncovalent polypseudorotaxane G⊂CB[8] and PSS can not only further dramatically boost the original phosphorescent emission by forming tight nanoparticle but also provide a scaffold to realize efficient long-lived NIR delayed fluorescence via RTP energy transfer after introduction of organic dye Rhodamine 800 (Rh800) as an acceptor. Intriguingly, the obtained system exhibited high response capability to antibiotics and was successfully applied NIR imaging antibiotics in living cells.

RESULTS AND DISCUSSION

The molecular structure and the synthetic route of guest molecules G and G_{re} were described in Schemes S1−S2, which were then fully characterized by high-resolution mass spectrometry (HR-MS) and nuclear magnetic resonance (NMR) (Figures S1−S6). The 4-(4-bromophenyl)-pyridine derivatives were chosen as phosphors where their N-termini were bridged by diverse lengths of aliphatic chain to obtain the dicationic dumbbell-shaped structure, which was anticipated that they could be endowed with differentiated amphiphilic features and host−guest assembled modes with CB[8]. First, ^{1}H NMR titration experiments were conducted to detailedly investigate the host−guest binding behaviors for G_{re} or G with CB[8]. As depicted from Figure S7, the proton signals ($H_{a'}$−$H_{d'}$) of the aromatic moiety in G_{re} obviously shifted upfield with 0.14, 0.49, 1.92, and 2.11 ppm respectively attributed to the shielding effect, whereas the chemical shifts of aliphatic protons of $H_{e'}$−$H_{f'}$ basically remained unchanged and that of $H_{g'}$ displayed a slight upfield shift upon the continuous addition of CB[8] to 1.0 equiv. Moreover, it can be distinctly distinguished both free and bound guest molecules on the ^{1}H NMR time scale on account of the slow exchange equilibria for the molecular recognition. Furthermore, all proton signals of G_{re} no longer changed in the presence of excess CB[8] above1.0 equiv, describing a 1:1 host−guest binding stoichiometry for G_{re} with CB[8]. Notably, the H_α and H_β of CB[8] on the exterior portals clearly split into two sets of equivalent groups, suggesting the different magnetic environments for two portals of CB[8] resulting from the unsymmetrical inclusion of the G_{re} inside the cavity. These phenomena jointly implied that the aromatic rings were exclusively incorporated into the CB[8] cavity according to the head-to-head and molecular folding mode, while the aliphatic chain linkers was located outside the cavity, which was consistent with the previous report.[51−53] However, G showed a completely different ^{1}H NMR titration result with CB[8] compared to G_{re}. As discerned in Figure 1a and Figure S8, both

https://doi.org/10.1021/jacsau.3c00642
JACS Au XXXX, XXX, XXX−XXX

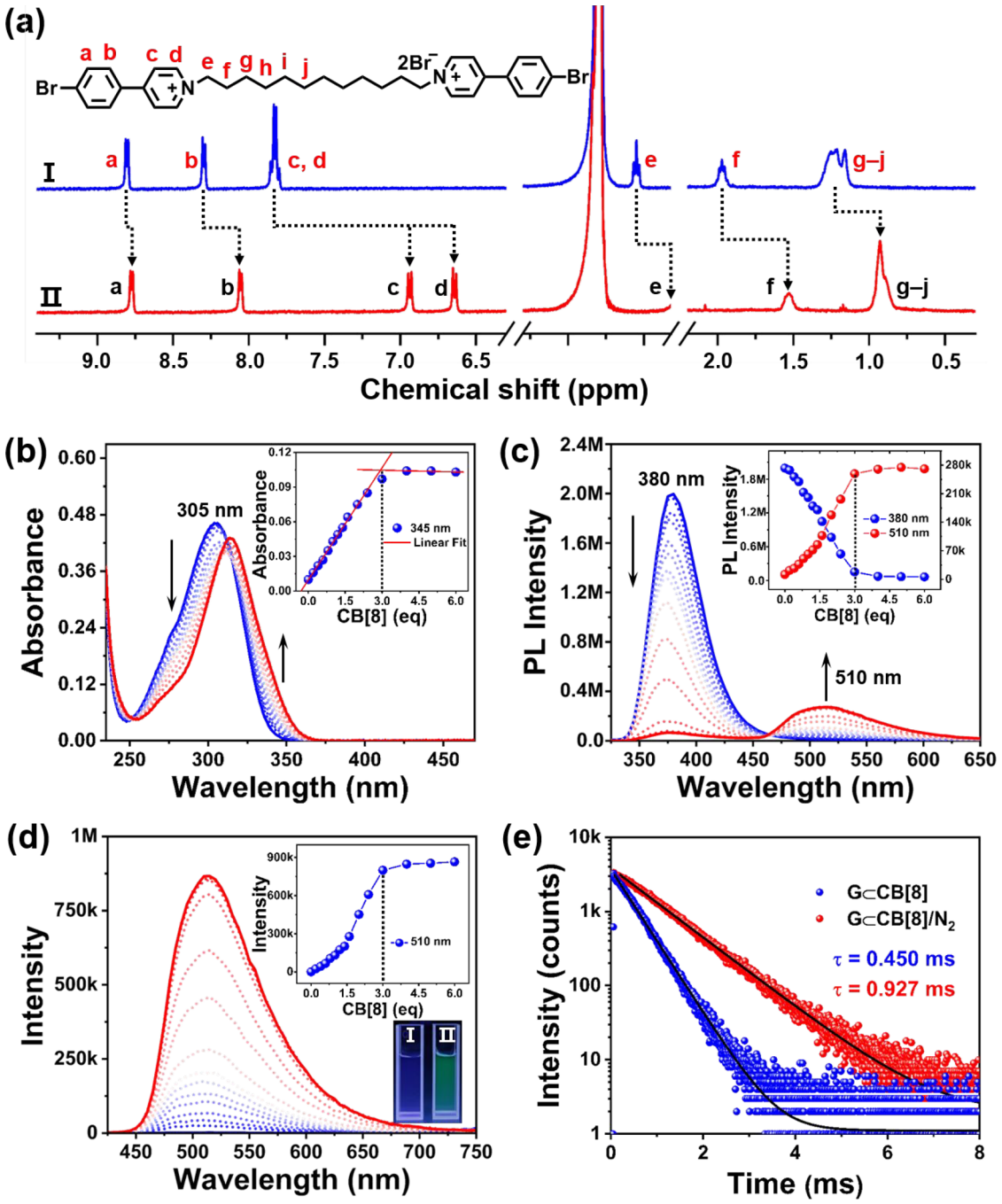

Figure 1. (a) Partial ^{1}H NMR spectra (400 MHz, D_2O, 298 K) of G ([G] = 1.0×10^{-4} M) upon addition with (I) 0 and (II) 3.0 equiv of CB[8]. (b) UV−vis absorption spectra and (inset) the corresponding absorbance intensity changes of G at 345 nm upon the gradual addition of CB[8] in aqueous solution ([G] = 1.0×10^{-5} M and [CB[8]] = 0−6.0×10^{-5} M). (c) Prompt photoluminescence spectra and (inset) the corresponding photoluminescence emission intensity changes of G at 380 and 510 nm in the presence of CB[8] in aqueous solution ([G] = 1.0×10^{-5} M and [CB[8]] = 0−6.0×10^{-5} M, λ_{ex} = 315 nm). (d) Phosphorescence emission spectra (delay = 50 μs) and (inset) the corresponding emission intensity changes of G at 510 nm in the presence of CB[8] in aqueous solution at ([G] = 1.0×10^{-5} M and [CB[8]] = 0−6.0×10^{-5} M, λ_{ex} = 315 nm). Photographic images of (I) free G and (II) G⊂CB[8] upon exposed to UV light under ambient conditions. (e) Time-resolved photoluminescence decay spectra of G⊂CB[8] at 510 nm (λ_{ex} = 315 nm) before and after N_2 bubbling in aqueous solution at 298 K.

the aromatic proton signals of bromophenylpyridine moieties (H_a−H_d) and dodecyl chain (H_e−H_j) all gradually shifted to the upfield due to the shielding effect upon addition of CB[8] from 0 to 1.0 equiv, indicative of the quick shuttle process of CB[8] on G and the fast exchange equilibria dynamics for the molecular recognition between them. When subsequently increasing the amount of CB[8] to 2.0 equiv, all proton signals of G continued to move upfield shifts, meaning that there are two CB[8] molecules over G at this stage. During the further addition of CB[8] from 2.0 to 3.0 equiv, the slow exchange equilibria in the CB[8]-involved molecular recognition process could be observed. Interestingly, all proton signals of G presented unchanged chemical shifts and reached the equilibrium state when the amount of CB[8] increased to >3.0 equiv, validating that G was thoroughly encapsulated into the rigid cavity of CB[8] with a 1:3 binding stoichiometry

https://doi.org/10.1021/jacsau.3c00642
JACS Au XXXX, XXX, XXX−XXX

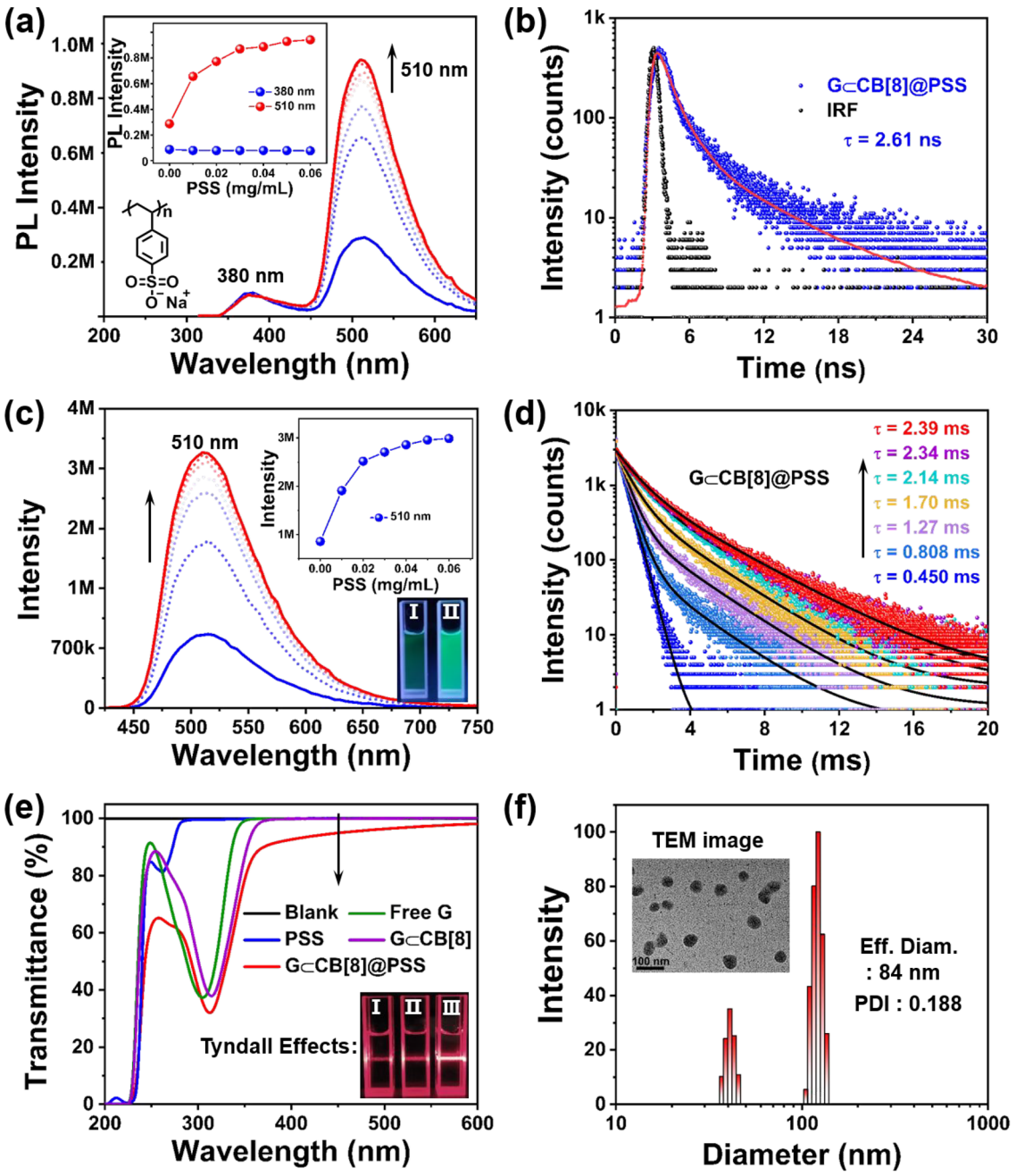

Figure 2. (a) Prompt photoluminescence spectra and (inset) the corresponding photoluminescence emission intensity changes of G⊂CB[8] at 380 and 510 nm in the presence of PSS in aqueous solution ([G] = 1.0×10^{-5} M, [CB[8]] = 3.0×10^{-5} M, and [PSS] = 0−0.06 mg/mL, λ_{ex} = 315 nm). (b) Time-resolved photoluminescence decay spectrum of G⊂CB[8]@PSS at 380 nm (λ_{ex} = 315 nm) in aqueous solution at 298 K. (c) Phosphorescence emission spectra (delay = 50 μs) and (inset) the corresponding emission intensity changes of G⊂CB[8] at 510 nm in the presence of PSS in aqueous solution ([G] = 1.0×10^{-5} M, [CB[8]] = 3.0×10^{-5} M, and [PSS] = 0−0.06 mg/mL, λ_{ex} = 315 nm). Photographic images of (I) G⊂CB[8] and (II) G⊂CB[8]/PSS upon exposed to UV light under ambient conditions. (d) Time-resolved photoluminescence decay spectra of G⊂CB[8] at 510 nm (λ_{ex} = 315 nm) upon the gradual addition of PSS ([PSS] = 0−0.06 mg/mL) in aqueous solution at 298 K. (e) Optical transmittance of G, G⊂CB[8], and G⊂CB[8]@PSS at 450 nm and (inset) the corresponding Tyndall effects in aqueous solution. (f) Dynamic light scattering analysis and (inset) transmission electron microscopy image of G⊂CB[8]@PSS assembly.

mode. Also, strong ROE correlations were observed between H_β and H_f−H_j protons (Figure S9), indicating that the dodecyl substituent simultaneously docked to CB[8] through hydrophobic interactions as well as cation−dipole interactions between the portal oxygen atoms of CB[8] and pyridinium nitrogen atoms of G,[54−58] thereby contributing to the formation of linear polypseudorotaxane.

Next, the complexation-induced changes of photophysical properties for G_{re} and G were examined by means of UV−vis absorption spectroscopy and photoluminescence spectroscopy in aqueous solution, respectively. As seen in Figure S10, upon the stepwise addition of CB[8] into aqueous solution of G_{re}, the absorbance intensity of G_{re} at 305 nm showed a significant decline accompanied by an obvious bathochromic shift to 311 nm and the appearance of an isosbestic point at 324 nm. On

https://doi.org/10.1021/jacsau.3c00642
JACS Au XXXX, XXX, XXX−XXX

the basis of the changes in absorption intensity at 305 nm using a nonlinear least-squares method, the association constant (K_s) for G_{re}⊂CB[8] was calculated to be 1.41 × 10^7 M^{-1} (Figure S10, inset). For G, the absorbance peak of G at 305 nm gradually decreased and underwent a red shift to 315 nm during the addition of CB[8] from 0 to 6.0 equiv. The curve of complexation-induced changes of absorbance intensity at 345 nm versus equivalents of CB[8] showed an inflection point at 3.0, also revealing a 1:3 binding stoichiometry between G and CB[8] corresponding to the ^{1}H NMR titration result (Figure 1b). In the photoluminescence spectra, the free G gave a single emission peak at 380 nm in aqueous solution; however, this emission dramatically declined upon the upon stepwise titration with CB[8] accompanied by an appeared emission peak at 510 nm with simultaneous increase in intensity (Figure 1c). It could be observed that the emission intensity in both 380 and 510 nm almost reached a plateau at 3.0 equiv of CB[8], which was consistent with the result of UV−vis titration experiment (Figure 1c, inset). The photoluminescent changes can also be recognized by the naked eye, wherein the initial blue color of G was converted to green after complexation with CB[8] under illumination with UV light (Figure 1d, inset). Moreover, the long-life and short-life emission natures of emission peaks at 510 and 380 nm could be readily distinguished from the time-gated emission spectra (delay time = 50 μs) (Figure S11). In addition, time-gated emission spectrum also uncovered that an intense peak centered on 510 nm gradually emerged upon the titration of G with continuous addition of CB[8] which almost achieved an equilibrium at 3.0 equiv of CB[8] (Figure 1d). The time-resolved PL decay curves showed that the lifetimes at 380 and 510 nm were measured as nanosecond-scale 2.21 ns and millisecond-level 0.450 ms under ambient conditions, where the lifetime at 510 nm could be markedly elongated to 0.927 ms upon deoxygenating the solution with nitrogen (N_2) due to the protection of triplet state of the phosphor from quenching, suggesting that these two peaks are attributed to typical fluorescence emission and macrocyclic confinement-induced room-temperature phosphorescence, respectively (Figure 1e and Figure S12). Similar photoluminescent behaviors could be found for the case of G_{re} during the titration with CB[8] except for the different CB[8]-confined host−guest inclusion modes, where the phosphorescence lifetime at 510 nm was a little shorter than that of G⊂CB[8] (0.395 ms vs 0.450 ms), also in turn illustrating that the linear polypseudorotaxane structure was more favorable to generating effective room-temperature phosphorescence (Figures S13−S15). Combined with the results of the spectral titration and NMR experiments above, it can be inferred that the two pyridinium units were adopted as head-to-tail stacking mode in the cavity of CB[8] favored by CB[8]-stabilized charge-transfer interactions, where the confinement effect from rigid cavity of CB[8] could result in the valid immobilization of the phosphor and reduction of nonradiative relaxation attenuation thus finally producing phosphorescence emission.

Recently, the oppositely charged functional macrocycles has been shown to further coassemble with well-defined host−guest pairs and then improve their original luminescence performance.[59−61] To this end, poly(4-styrene-sulfonic sodium) (PSS), as an anionic material, was first utilized to further interact with positively multicharged G⊂CB[8] polypseudorotaxane for constructing high-performance phosphorescent assembly in aqueous solution. As depicted in Figure 2a, the phosphorescence intensity at 510 nm sharply increased when PSS was gradually added into an aqueous solution of G⊂CB[8], which remained nearly balanced at the PSS concentration of 0.06 mg/mL. However, the fluorescence intensity at 380 nm almost kept constant in this process and exhibited a final lifetime of 2.61 ns (Figure 2b). The time-gated emission spectra also showed similar results, where the previous phosphorescence intensity was enhanced approximately four times with a dramatic increase in phosphorescence quantum yield from 1.13% to 13.16% and the aqueous solution of G⊂CB[8]@PSS showed a more intense green phosphorescence than G⊂CB[8] under UV light (Figure 2c). The normalized photoluminescence spectra for G, G_{re}, G_{re}⊂CB[8], G⊂CB[8], and G⊂CB[8]@PSS were shown in Figure S16.

Furthermore, the change of phosphorescence lifetimes at 510 nm after adding different PSS into G solution was also monitored, revealing that the phosphorescence lifetime increasingly extended from the earliest 0.450 to 2.39 ms with the stepwise addition of PSS (Figure 2d). Interestingly, the PSS alone and the direct assembly of G with PSS could hardly produce any phosphorescence in aqueous solution, thereby confirming the indispensable role of the CB[8]-confined effect for inducing phosphorescence generation (Figure S17). Importantly, these results illustrated that the addition of PSS did contribute to the great improvement on phosphorescence performance instead of disrupting the G⊂CB[8] polypseudorotaxane. In comparison, the phosphorescence intensity of loop structure G_{re}⊂CB[8] demonstrated a decreasing trend after the interaction with PSS and the original lifetime was reduced from 0.395 to 0.305 ms (Figures S18 and S19). These phenomena consistently demonstrated that the linear polypseudorotaxane structure of G⊂CB[8] was more conducive to secondarily assembling with PSS driven by synergistic noncovalent interactions, which ultimately further suppressed nonradiative decay processes and effectively shielded the phosphor within the formed multivalent assembly from attack of quenchers like dissolved oxygen species to yield excellent phosphorescence property.

In addition, the changes of optical transmittance were also monitored to gain more insight on the assembly process between PSS and G⊂CB[8]. As seen in Figure 2e, by using pure water as a reference sample, it was found that neither G, PSS, nor G⊂CB[8] showed any optical transmittance changes, while the subsequent interaction with PSS led to the sharp decline for the optical transmittance of G⊂CB[8] at 450 nm, signifying the formation of large nanoconstructs benefiting from the electrostatic interaction between them. Analogously, in contrast to free G and G⊂CB[8], the most conspicuous Tyndall effect could be easily distinguished for G⊂CB[8]@PSS (Figure 2e, inset). The specific morphologic information on G⊂CB[8]@PSS assemblies was next probed in detail via dynamic light scattering (DLS), zeta potential experiments, and transmission electron microscopy (TEM). DLS test provided the average hydrodynamic diameter of G⊂CB[8]@PSS assemblies as 84 nm with a narrow size distribution (Figure 2f). Besides, the average zeta potential of G⊂CB[8] was measured to be +19.67 mV, while that of G⊂CB[8]@PSS was −15.54 mV, indicating the negatively charged surface of multivalent coassembly after the addition of PSS (Figure S20). TEM images revealed that free G was recognized as some irregular small-sized aggregates, while G⊂CB[8] existed as one-dimensional linear nanofibers with lengths on the micron scale, directly confirming the formation of supramolecular

https://doi.org/10.1021/jacsau.3c00642
JACS Au XXXX, XXX, XXX−XXX

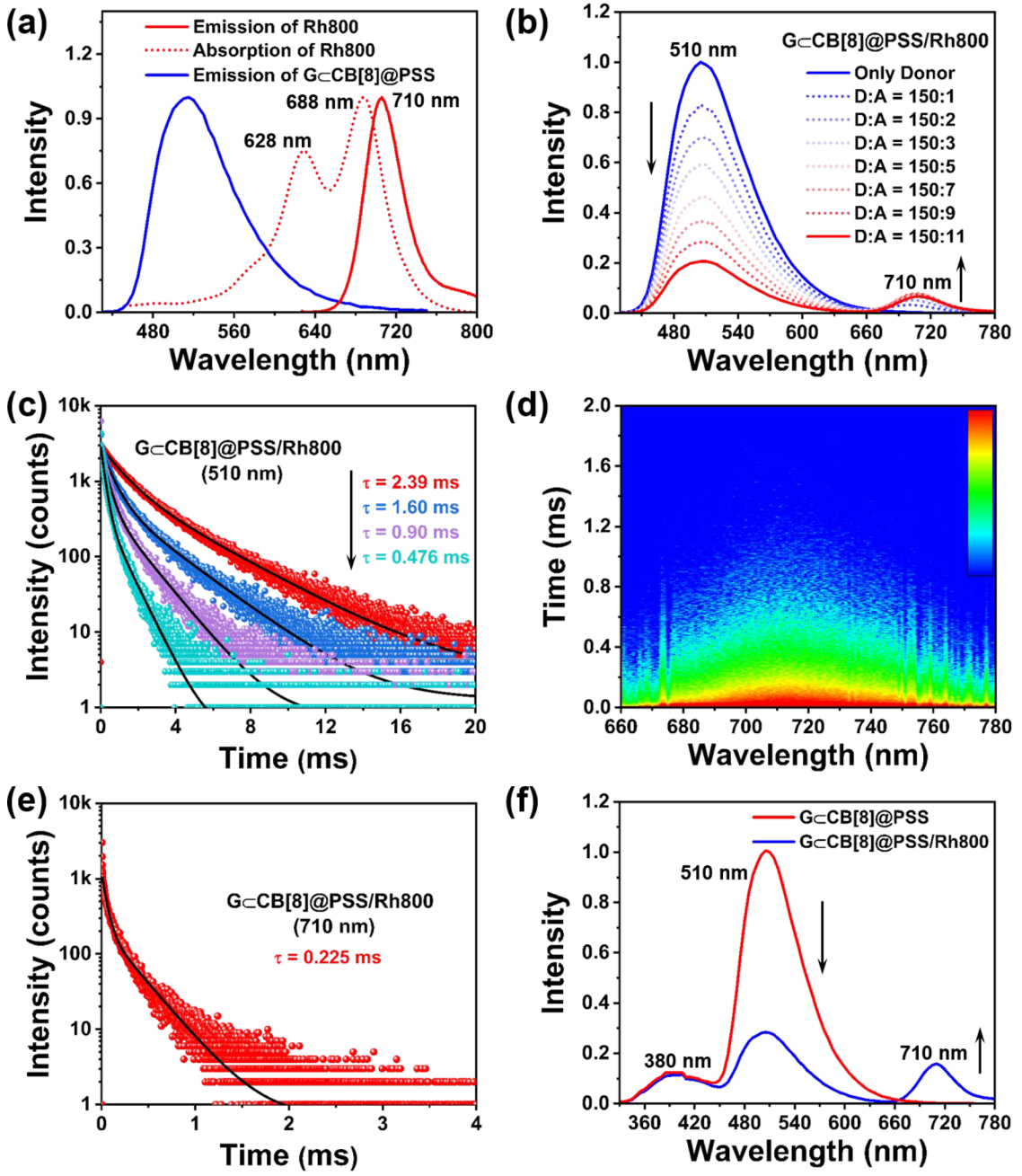

Figure 3. (a) Normalized absorption and emission spectra of Rh800 and the phosphorescence emission spectrum of G⊂CB[8]@PSS assembly in aqueous solution. (b) Phosphorescence emission spectra (delay = 50 μs) of G⊂CB[8]@PSS/Rh800 at different donor/acceptor ratios in aqueous solution ([G] = 1.0×10^{-5} M, [CB[8]] = 3.0×10^{-5} M, and [PSS] = 0.06 mg/mL, λ_{ex} = 315 nm). (c) Time-resolved photoluminescence decay spectra of G⊂CB[8]@PSS/Rh800 at 510 nm (λ_{ex} = 315 nm) with the donor/acceptor ratio of 150:3, 150:7 and 150:11 in aqueous solution at 298 K. (d) Time-resolved phosphorescence emission mapping of G⊂CB[8]@PSS/Rh800 at the donor/acceptor ratio of 150:11 in aqueous solution at 298 K (λ_{ex} = 315 nm). (e) Time-resolved photoluminescence decay spectra of G⊂CB[8]@PSS/Rh800 at 710 nm (λ_{ex} = 315 nm) in aqueous solution at 298 K. (f) Prompt photoluminescence spectral changes of G⊂CB[8]@PSS upon the addition of Rh800 at the donor/acceptor ratio of 150:11 in aqueous solution.

polypseudorotaxane (Figure S21). Moreover, G⊂CB[8]@PSS showed distinctly different structural features with G⊂CB[8], where a number of homogeneous near-spherical nanoparticles with a diameter of ca. 50 nm were observed basically consistent with the DLS result (Figure 2f, inset). These results jointly demonstrated that PSS can definitely participate in the further coassembly process with the linear supramolecular polypseudorotaxane G⊂CB[8] to form uniform tight nanoparticles facilitated by electrostatic interactions.

Considering the excellent phosphorescence emission properties and the favorable nanoparticle structure of the coassemblies, we wonder if it could serve as an artificial light-harvesting scaffold to perform the phosphorescent energy transfer process via tertiary assembly driven by multivalent interactions by loading suitable organic dye into their interior hydrophobic environment with the shortened distance with antenna phosphors. In the present case, Rh800, as a positively charged NIR emissive organic dye, was chosen as the acceptor

https://doi.org/10.1021/jacsau.3c00642
JACS Au XXXX, XXX, XXX−XXX

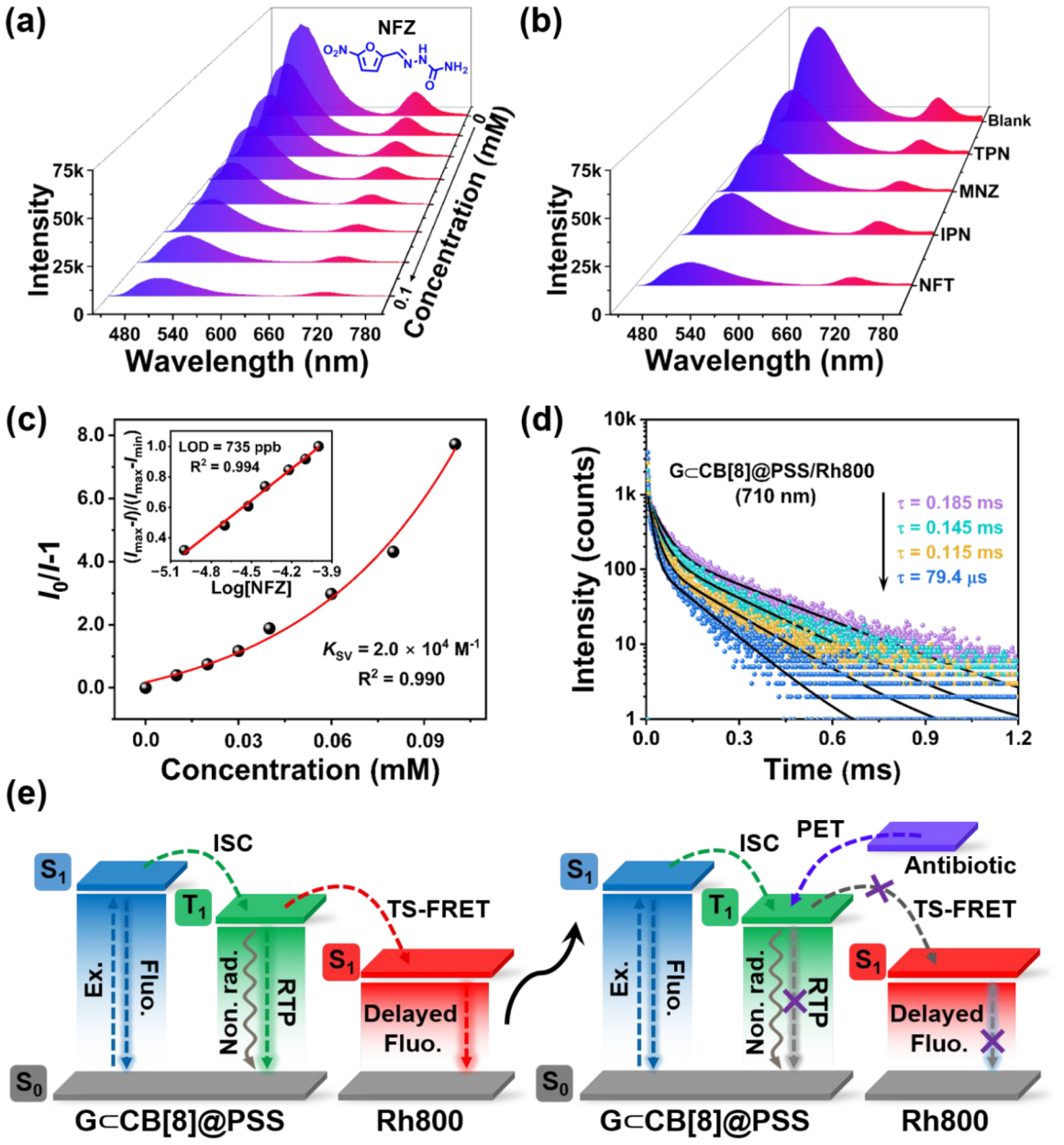

Figure 4. (a) Phosphorescence emission spectra (delay = 50 μs) of G⊂CB[8]@PSS/Rh800 upon the gradual addition of 0, 0.01, 0.02, 0.03, 0.04, 0.06, 0.08, and 0.10 mM NFZ ([G] = 1.0×10^{-5} M, [CB[8]] = 3.0×10^{-5} M, [PSS] = 0.06 mg/mL, and [Rh800] = 7.3×10^{-7} M, λ_{ex} = 315 nm). (b) Phosphorescence emission spectra (delay = 50 μs) of G⊂CB[8]@PSS/Rh800 toward various antibiotics with concentration of 0.10 mM in aqueous solution. (c) Stern−Volmer plot of G⊂CB[8]@PSS/Rh800 and (inset) $(I_{max} - I)/(I_{max} - I_{min})$ vs Log[NFZ] plot at different concentrations of NFZ. (d) Time-resolved photoluminescence decay spectra of G⊂CB[8]@PSS/Rh800 at 710 nm (λ_{ex} = 315 nm) upon the addition of 1.0, 3.0, 6.0, and 10.0 equiv of NFZ in aqueous solution at 298 K. (e) Graphical possible working mechanism for the phosphorescence energy transfer process and antibiotic sensing.

owing to the valid spectral overlap between the absorption band of Rh800 and phosphorescence emission band of G⊂CB[8]@PSS ensuring the feasibility of energy transfer (Figure 3a). As illustrated in Figure 3b, in the time-gated spectra, the gradual addition of RB800 with the donor/acceptor ratio ranging from 150:1 to 150:11 into the aqueous solution of G⊂CB[8]@PSS coassembly, led to the significant quenching of initial phosphorescence intensity at 510 nm, whereas an emerging NIR emission intensity at 710 nm increased accordingly. However, free RB800 emitted negligible emission with the absence of G⊂CB[8]@PSS in the gated spectra under the same conditions, indicating that G⊂CB[8]@PSS directly contributed to the amplified NIR signal (Figure S22). Particularly, the NIR emission peak of G⊂CB[8]@PSS/Rh800 system displayed a same maximum emission wavelength (675 nm) with the fluorescence of free Rh800, which meant this NIR emission belonged to the characteristic delayed fluorescence emission. These results suggested the phosphorescence energy transfer indeed took place from the triplet state of the phosphors to the singlet state of Rh800 within the coassemblies. Moreover, the changes of lifetimes in this process were also elaborately studied from the time-resolved decay measurements to elucidate the mechanism, which showed that the phosphorescence lifetime at 510 nm gradually

https://doi.org/10.1021/jacsau.3c00642
JACS Au XXXX, XXX, XXX−XXX

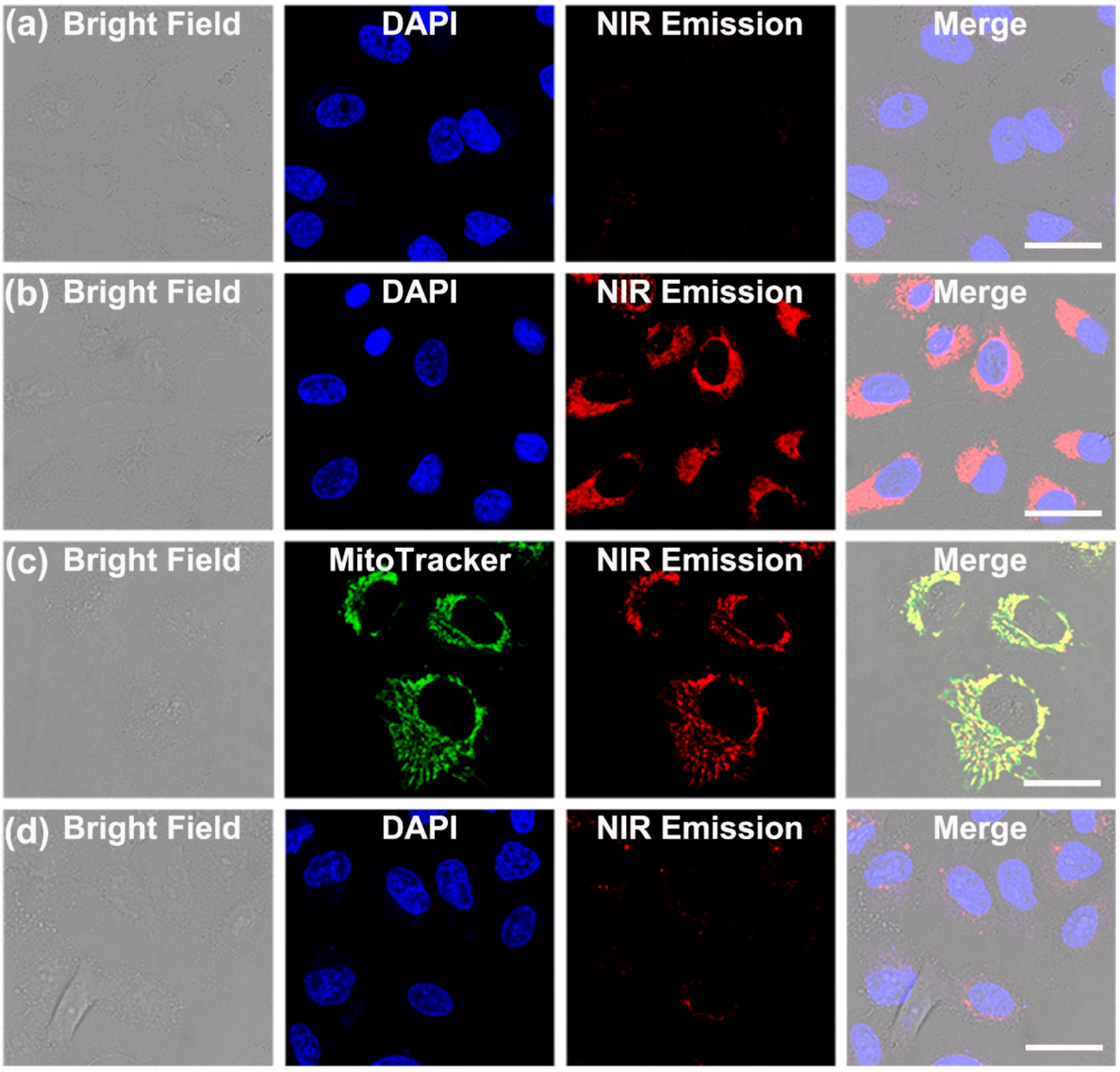

Figure 5. Cellular imaging of A549 cancer cells stained with (a) free Rh800 and (b) G⊂CB[8]@PSS/Rh800 coassembly ([G] = 5.0×10^{-6} M, [CB[8]] = 1.5×10^{-5} M, [PSS] = 0.03 mg/mL, and [Rh800] = 3.7×10^{-7} M). (c) Mitochondria colocalization images in living A549 cancer cells. (d) Cellular imaging of A549 cancer cells costained with G⊂CB[8]@PSS/Rh800 coassembly and NFZ ([G] = 5.0×10^{-6} M, [CB[8]] = 1.5×10^{-5} M, [PSS] = 0.03 mg/mL, [Rh800] = 3.7×10^{-7} M, and [NFZ] = 5.0×10^{-6} M). 4,6-Diamidino-2-phenylindole (DAPI, blue) and MitoTracker Green were utilized to stain the nuclei and mitochondria, which were observed from 420 to 470 nm and from 500 to 550 nm, respectively. The NIR channel was observed from 700 to 800 nm (Scale bar = 25 μm).

reduced from 2.39 to 0.436 ms upon the continuous addition of Rh800 (Figure 3c), further validating the nonradiative triplet-to-singlet Förster resonance energy transfer (TS-FRET) mechanism instead of the radiative energy transfer mechanism.[62,63] Meanwhile, according to the decreased phosphorescence lifetime, the energy transfer efficiency was calculated as 80.1% at a donor/acceptor ratio of 150:11. Notably, the time-resolved phosphorescence emission mapping revealed the main long-lived emission band centered on 710 nm after energy transfer process (Figure 3d). And the lifetime of the appeared emission at 710 nm in the gated spectra was determined as millisecond-scaled 0.225 ms (Figure 3e), while that of free Rh800 was measured as 3.27 ns in the order of nanoseconds (Figure S23). Additionally, there was no apparent changes of intensity for the fluorescence emission of G⊂CB[8]@PSS after the addition of Rh800, which proved that the short-lived fluorescent component was not involved in the singlet−singlet FRET process because of the poorly spectral overlap between them (Figure 3f). These results clearly illustrated that an efficient NIR phosphorescence-harvesting system was successfully obtained in aqueous solution by doping a small amount of Rh800 acceptors into assemblies, taking advantage of the triplet to singlet FRET based on the delayed sensitization process.

It has been reported that the short-lived fluorescence-based supramolecular artificial light-harvesting systems can act as probes for optical sensing, however, the phosphorescence-based ones with longer lifetime to achieve above goal is still rare. For this purpose, the commonly used antibiotics including nitrofurazone (NFZ), sulfamethazine (SMZ), nitrofurantoin (NFT), imipenem (IPN), thiamphenicol (TPN), and metronidazole (MNZ), were employed as analytical

https://doi.org/10.1021/jacsau.3c00642
JACS Au XXXX, XXX, XXX−XXX

substrates to investigate the sensing capability of G⊂CB[8]@PSS/Rh800 (Figure S24). Remarkably, a considerable quenching performance on coassembly was evidently found, where the original signal intensity obviously declined upon the incremental concentration of NFZ or SMZ from 0 to 10 equiv (Figure 4a and Figure S25). The quenching efficiency was determined exactly by the ratio of the change in the emission intensity to the initial value $[(I_0 - I)/I_0]$ at 710 nm. As judged from Figure 4b, other analytes also exhibited a certain extent quenching effect on the emission of coassembly especially for the NIR emission at 710 nm. The calculated quenching efficiencies were in the following order: NFZ (88.5%) > SMZ (87.9%) > NFT (74.3%) > MNZ (60.1%) > IPN (55.0%) > TPN (43.1%), respectively. In addition, the sensing capabilities of coassembly toward NFZ and SMZ were quantitatively evaluated by the Stern−Volmer relationship. The final quenching constants (K_{SV}) and the limit of detection (LOD) values were respectively calculated as 2.0×10^4 M^{-1} and 735 ppb for NFZ and 7.6×10^3 M^{-1} and 934 ppb for SMZ, hinting a strong quenching behavior to coassembly luminescence (Figure 4c and Figure S26). However, it was found that the free Rh800 without G⊂CB[8]@PSS did not express any sensing ability to NFZ or SMZ (Figures S27 and S28), indicating that the quenching NIR emission originated from the cutoff of pathway in TS-FRET process. The UV−vis absorption of antibiotics showed no significant changes after the addition of CB[8], suggesting that the guest G was not expelled from the cavity of CB[8] due to competitive binding of antibiotics (Figure S29). To further investigate the emission quenching mechanism, the emission lifetimes (τ) after adding different concentrations of analyte were measured by taking NFZ as an example. As shown in Figure 4d and Figure S30, the long lifetime of NIR emission at 710 nm decreased progressively to 79.4 μs when increasing the concentration of NFZ; meanwhile, the phosphorescence lifetime at 510 nm also sharply dropped from 0.476 to 0.268 ms. It was worth noting that the fitting of $1/\tau$ vs [NFZ] showed a good linear relationship which was consistent with a typical diffusion-controlled electron transfer reaction (Figure S31).[64,65] Therefore, the quenching mechanism was probably caused by the photoinduced electron transfer (PET) from antibiotics to the excited state of G⊂CB[8], eventually resulting in the phosphorescence quenching and the prohibition of TS-FRET process. The possible working mechanism for the phosphorescence energy transfer and subsequent antibiotic sensing was presented in Figure 4e. These results clearly demonstrated that the constructed NIR emissive phosphorescence-harvesting system possessing an excellent potential detection capability can be utilized as a sensor material to monitor antibiotics in aqueous solution.

Therefore, the remarkable long-lived NIR emission behavior of the obtained coassembly motivated us to further explore its potential application in cellular imaging and the corresponding antibiotics-sensing capability in cells. The cytotoxicity of this system was first assessed in a concentration-dependent manner using the human lung adenocarcinoma cells (A549 cells). The results of standard cell counting kit (CCK)-8 assay demonstrated that such system displayed a very low toxicity and the cell viability remained more than 91% after 24 h incubation within 30 μM (Figure S32). Subsequently, confocal laser scanning microscopy was used to visualize the intracellular NIR emission signal. As depicted in Figure 5a,b, it could be clearly observed that the cells after treatment with G⊂CB[8]@PSS/Rh800 coassembly presented a fairly bright red emission signal evenly distributed around the nucleus, whereas the Rh800 itself only emitted a negligible emission signal in NIR channel, indicative of the phosphorescence energy transfer enhanced NIR delayed emission. Moreover, colocalization experiment was also performed to further clarify subcellular localization of coassembly by using a commercial mitochondria marker MitoTracker Green. It could be judged from the yellow areas in the overlapped image that the coassemblies were predominately located at mitochondria with a relatively high Pearson's correlation coefficient as 0.82 (Figure 5c and Figure S33). In keen contrast, after the cells treatment with NFZ, the original bright red signal almost ignorable under the same experimental conditions, illuminating that NFZ could significantly quench the delayed NIR emission signal in the cellular environment (Figure 5d).

CONCLUSIONS

In conclusion, a high-efficiency phosphorescence resonance energy transfer assembly is successfully fabricated in water from dodecyl-chain-bridged 4-(4-bromophenyl)-pyridine derivative (G), cucurbit[8]uril (CB[8]), and poly(4-styrenesulfonic sodium) (PSS) in aqueous solution, which not only realized efficient aqueous phosphorescence at 510 nm but also finally achieved long-lived near-infrared (NIR) delayed fluorescence emission at 710 nm after tertiary assembly with Rhodamine 800. By virtue of the effective hierarchical confinement toward G resulting from CB[8] and PSS, the polypseudorotaxane assembly G⊂CB[8]@PSS exhibited considerable enhancement of phosphorescence performance and can served as capturing platform to perform phosphorescence energy transfer after doping a small amount of Rhodamine 800. Importantly, the obtained system presented efficient capability responding to antibiotics, thereby making it a suitable candidate for NIR sensing antibiotics in living cells. This study not only provides a simple and feasible method for the construction of long-lived NIR emission materials in the aqueous phase but also implies the possibility of employing them as chemical sensors in biological environment, which has great potential value in supramolecular diagnosis and treatment research.

METHODS

Synthesis of Compound G_{re}

1,6-Dibromohexane (1.0 mmol, 244 mg, 1.0 equiv) and 4-(4-bromophenyl)-pyridine (3.0 mmol, 585 mg, 2.5 equiv) were dissolved in anhydrous CH_3CN (15 mL). After reacting at 85 °C for 24 h under N_2 atmosphere, the reaction was cooled to room temperature. Subsequently, a large amount of precipitate was deposited, and filtered to get solid then the product was washed with CH_3CN and diethyl ether to obtain compound G_{re} (yield: 72%). ^{1}H NMR (400 MHz, DMSO-d_6, ppm) δ 9.19 (d, J = 6.7 Hz, 2H), 8.56 (d, J = 6.8 Hz, 2H), 8.05 (d, J = 8.6 Hz, 2H), 7.86 (d, J = 8.6 Hz, 2H), 4.62 (t, J = 7.3 Hz, 2H), 1.95 (s, 2H), 1.36 (s, 2H); ^{13}C NMR (100 MHz, DMSO-d_6, ppm) δ 153.45 (s), 144.89 (s), 132.71 (s), 132.63 (s), 130.15 (s), 126.23 (s), 124.47 (s), 59.73 (s), 30.29 (s), 24.78 (s); HRMS (ESI): m/z calcd for $C_{28}H_{28}Br_2N_2^+$ 275.0304 $[M - 2Br^-]^{2+}/2$; found: 275.0311.

Synthesis of Compound G

1,12-Dibromododecane (1.0 mmol, 328 mg, 1.0 equiv) and 4-(4-bromophenyl)-pyridine (3.0 mmol, 585 mg, 2.5 equiv) were dissolved in anhydrous CH_3CN (15 mL). After reacting at 85 °C for 24 h under N_2 atmosphere, the reaction was cooled to room temperature.

https://doi.org/10.1021/jacsau.3c00642
JACS Au XXXX, XXX, XXX−XXX

Subsequently, a large amount of precipitate was deposited, and filtered to get solid then the product was washed with CH_3CN and diethyl ether to obtain compound G (yield: 63%). ^{1}H NMR (400 MHz, DMSO-d_6, ppm) δ 9.13 (d, J = 6.7 Hz, 2H), 8.54 (d, J = 6.7 Hz, 2H), 8.04 (d, J = 8.6 Hz, 2H), 7.87 (d, J = 8.6 Hz, 2H), 4.57 (t, J = 7.3 Hz, 2H), 1.92 (s, 2H), 1.25 (d, J = 17.3 Hz, 8H); ^{13}C NMR (100 MHz, DMSO-d_6, ppm) δ 153.46 (s), 144.70 (s), 132.73 (s), 132.64 (s), 130.14 (s), 126.23 (s), 124.43 (s), 59.97 (s), 30.63 (s), 28.94 (s), 28.84 (s), 28.46 (s), 25.46 (s); HRMS (ESI): m/z calcd for $C_{34}H_{40}Br_2N_2^{2+}$ 317.0774 $[M - 2Br^-]^{2+}/2$; found: 317.0775.

■ ASSOCIATED CONTENT

Supporting Information

The Supporting Information is available free of charge at https://pubs.acs.org/doi/10.1021/jacsau.3c00642.

Detailed experiments included synthetic procedures and characterizations, and additional figures in the optical experiments for assemblies (PDF)

■ AUTHOR INFORMATION

Corresponding Author

Yu Liu − *College of Chemistry, State Key Laboratory of Elemento-Organic Chemistry, Nankai University, Tianjin 300071, P. R. China;* orcid.org/0000-0001-8723-1896; Email: yuliu@nankai.edu.cn

Authors

Xian-Yin Dai − *School of Chemistry and Pharmaceutical Engineering, Shandong First Medical University & Shandong Academy of Medical Sciences, Taian, Shandong 271016, P. R. China;* orcid.org/0000-0002-1390-1823

Qi Song − *School of Chemistry and Pharmaceutical Engineering, Shandong First Medical University & Shandong Academy of Medical Sciences, Taian, Shandong 271016, P. R. China*

Wei-Lei Zhou − *College of Chemistry, State Key Laboratory of Elemento-Organic Chemistry, Nankai University, Tianjin 300071, P. R. China*

Complete contact information is available at: https://pubs.acs.org/10.1021/jacsau.3c00642

Author Contributions

X.-Y.D. conceived and designed the experiments. Q.S. synthesized and performed the chemical characterization. X.-Y.D. wrote the main manuscript. Y.L. supervised the work and edited the manuscript. All authors analyzed and discussed the results and reviewed the manuscript.

Notes

The authors declare no competing financial interest.

■ ACKNOWLEDGMENTS

This work was financially supported by the Natural Science Foundation of Shandong Province (ZR2023QB186), the National Natural Science Foundation of China (22301166, 22131008 and 22101143).

■ REFERENCES

(1) Chen, X. M.; Cao, K. W.; Bisoyi, H. K.; Zhang, S.; Qian, N.; Guo, L.; Guo, D. S.; Yang, H.; Li, Q. Amphiphilicity-Controlled Polychromatic Emissive Supramolecular Self-Assemblies for Highly Sensitive and Efficient Artificial Light-Harvesting Systems. *Small* **2022**, *18*, No. e2204360.

(2) Das, R. S.; Saha, P. C.; Sepay, N.; Mukherjee, A.; Chatterjee, S.; Guha, S. Design and Synthesis of Near-Infrared Mechanically Interlocked Molecules for Specific Targeting of Mitochondria. *Org. Lett.* **2020**, *22*, 5839−5843.

(3) Jung, H. Y.; Kim, B.; Jeon, M. H.; Kim, Y. Reversible Near-Infrared Fluorescence Photoswitching in Aqueous Media by Diarylethene: Toward High-Accuracy Live Optical Imaging. *Small* **2022**, *18*, No. e2103523.

(4) Chen, X. M.; Cao, Q.; Bisoyi, H. K.; Wang, M.; Yang, H.; Li, Q. An Efficient Near-Infrared Emissive Artificial Supramolecular Light-Harvesting System for Imaging in the Golgi Apparatus. *Angew. Chem., Int. Ed.* **2020**, *59*, 10493−10497.

(5) Li, J.; Pu, K. Semiconducting Polymer Nanomaterials as Near-Infrared Photoactivatable Protherapeutics for Cancer. *Acc. Chem. Res.* **2020**, *53*, 752−762.

(6) Li, C.; Tu, L.; Yang, J.; Liu, C.; Xu, Y.; Li, J.; Tuo, W.; Olenyuk, B.; Sun, Y.; Stang, P. J.; Sun, Y. Acceptor engineering of metallacycles with high phototoxicity indices for safe and effective photodynamic therapy. *Chem. Sci.* **2023**, *14*, 2901−2909.

(7) Zhou, J.; Rao, L.; Yu, G.; Cook, T. R.; Chen, X.; Huang, F. Supramolecular cancer nanotheranostics. *Chem. Soc. Rev.* **2021**, *50*, 2839−2891.

(8) Wang, Y.; Wu, H.; Li, P.; Chen, S.; Jones, L. O.; Mosquera, M. A.; Zhang, L.; Cai, K.; Chen, H.; Chen, X. Y.; et al. Two-photon excited deep-red and near-infrared emissive organic co-crystals. *Nat. Commun.* **2020**, *11*, 4633.

(9) Baysec, S.; Minotto, A.; Klein, P.; Poddi, S.; Zampetti, A.; Allard, S.; Cacialli, F.; Scherf, U. Tetraphenylethylene-BODIPY aggregation-induced emission luminogens for near-infrared polymer light-emitting diodes. *Sci. China Chem.* **2018**, *61*, 932−939.

(10) Zhang, W.; Chen, S.; Ye, S.; Sun, P.; Fan, Q.; Song, J.; Zeng, P.; Qu, J.-L.; Wong, W.-Y. Enhancing NIR-II Phosphorescence through Phosphorescence Resonance Energy Transfer for Tumor-Hypoxia Imaging. *ACS Mater. Lett.* **2023**, *5*, 116−124.

(11) Zhao, M.; Li, B.; Zhang, H.; Zhang, F. Activatable fluorescence sensors for in vivo bio-detection in the second near-infrared window. *Chem. Sci.* **2021**, *12*, 3448−3459.

(12) Aryal, G. H.; Hunter, K. W.; Huang, L. A supramolecular red to near-infrared fluorescent probe for the detection of drugs in urine. *Org. Biomol. Chem.* **2018**, *16*, 7425−7429.

(13) Wang, H.; Ji, X.; Li, Z.; Huang, F. Fluorescent Supramolecular Polymeric Materials. *Adv. Mater.* **2017**, *29*, No. 1606117.

(14) Lou, X.-Y.; Yang, Y.-W. Manipulating Aggregation-Induced Emission with Supramolecular Macrocycles. *Adv. Opt. Mater.* **2018**, *6*, No. 1800668.

(15) Huang, Z.; Ma, X. Tailoring Tunable Luminescence via Supramolecular Assembly Strategies. *Cell Rep. Phys. Sci.* **2020**, *1*, No. 100167.

(16) Wang, Y.; Wu, H.; Hu, W.; Stoddart, J. F. Color-Tunable Supramolecular Luminescent Materials. *Adv. Mater.* **2022**, *34*, No. 2105405.

(17) Zhang, Q. W.; Li, D.; Li, X.; White, P. B.; Mecinovic, J.; Ma, X.; Agren, H.; Nolte, R. J. M.; Tian, H. Multicolor Photoluminescence Including White-Light Emission by a Single Host-Guest Complex. *J. Am. Chem. Soc.* **2016**, *138*, 13541−13550.

(18) Tu, C.; Wu, W.; Liang, W.; Zhang, D.; Xu, W.; Wan, S.; Lu, W.; Yang, C. Host−Guest Complexation-Induced Aggregation Based on Pyrene-Modified Cyclodextrins for Improved Electronic Circular Dichroism and Circularly Polarized Luminescence. *Angew. Chem., Int. Ed.* **2022**, *61*, No. e202203541.

(19) Chen, X. M.; Chen, Y.; Yu, Q.; Gu, B. H.; Liu, Y. Supramolecular Assemblies with Near-Infrared Emission Mediated in Two Stages by Cucurbituril and Amphiphilic Calixarene for Lysosome-Targeted Cell Imaging. *Angew. Chem., Int. Ed.* **2018**, *57*, 12519−12523.

(20) Lin, B.; Wang, Q.; Qi, Z.; Xu, H.; Qu, D.-H. Cucurbit[8]uril-mediated multi-color fluorescence system for time-dependent information encryption. *Sci. China Chem.* **2023**, *66*, 1111.

(21) Wang, Y.; Ma, C.-Q.; Li, X.-L.; Dong, R.-Z.; Liu, H.; Wang, R.-Z.; Yu, S.; Xing, L.-B. A novel strategy of constructing an artificial light-harvesting system based on a supramolecular organic framework for photocatalysis. *J. Mater. Chem. A* **2023**, *11*, 2627−2633.
(22) Yu, J.; Wang, H.; Dai, X.; Chen, Y.; Liu, Y. Multivalent Supramolecular Assembly Based on a Triphenylamine Derivative for Near-Infrared Lysosome Targeted Imaging. *ACS Appl. Mater. Interfaces* **2022**, *14*, 4417−4422.
(23) Shao, L.; Pan, Y.; Hua, B.; Xu, S.; Yu, G.; Wang, M.; Liu, B.; Huang, F. Constructing Adaptive Photosensitizers via Supramolecular Modification Based on Pillararene Host-Guest Interactions. *Angew. Chem., Int. Ed.* **2020**, *59*, 11779−11783.
(24) Shi, B.; Jie, K.; Zhou, Y.; Zhou, J.; Xia, D.; Huang, F. Nanoparticles with Near-Infrared Emission Enhanced by Pillararene-Based Molecular Recognition in Water. *J. Am. Chem. Soc.* **2016**, *138*, 80−83.
(25) Ahmed, S.; Kumar, A.; Mukherjee, P. S. Tetraphenylethene-Based Emissive Pt(II) Coordination Polymer toward Artificial Light-Harvesting Systems with Sequential Energy Transfer. *Chem. Mater.* **2022**, *34*, 9656−9665.
(26) Chen, X.-M.; Chen, X.; Hou, X.-F.; Zhang, S.; Chen, D.; Li, Q. Self-assembled supramolecular artificial light-harvesting nanosystems: construction, modulation, and applications. *Nanoscale Adv.* **2023**, *5*, 1830−1852.
(27) Wang, K.; Velmurugan, K.; Li, B.; Hu, X. Y. Artificial light-harvesting systems based on macrocycle-assisted supramolecular assembly in aqueous media. *Chem. Commun.* **2021**, *57*, 13641−13654.
(28) Xiao, T.; Bao, C.; Zhang, L.; Diao, K.; Ren, D.; Wei, C.; Li, Z.-Y.; Sun, X.-Q. *J. Mater. Chem. A* **2022**, *10*, 8528−8534.
(29) Xiao, T.; Zhong, W.; Zhou, L.; Xu, L.; Sun, X.-Q.; Elmes, R. B. P.; Hu, X.-Y.; Wang, L. Artificial light-harvesting systems fabricated by supramolecular host−guest interactions. *Chin. Chem. Lett.* **2019**, *30*, 31−36.
(30) Gao, R.; Kodaimati, M. S.; Yan, D. Recent advances in persistent luminescence based on molecular hybrid materials. *Chem. Soc. Rev.* **2021**, *50*, 5564−5589.
(31) Guo, J.; Yang, C.; Zhao, Y. Long-Lived Organic Room-Temperature Phosphorescence from Amorphous Polymer Systems. *Acc. Chem. Res.* **2022**, *55*, 1160−1170.
(32) Guo, S.; Dai, W.; Chen, X.; Lei, Y.; Shi, J.; Tong, B.; Cai, Z.; Dong, Y. Recent Progress in Pure Organic Room Temperature Phosphorescence of Small Molecular Host−Guest Systems. *ACS Mater. Lett.* **2021**, *3*, 379−397.
(33) Yan, X.; Peng, H.; Xiang, Y.; Wang, J.; Yu, L.; Tao, Y.; Li, H.; Huang, W.; Chen, R. Recent Advances on Host-Guest Material Systems toward Organic Room Temperature Phosphorescence. *Small* **2022**, *18*, No. e2104073.
(34) Yang, J.; Fang, M.; Li, Z. Stimulus-Responsive Room Temperature Phosphorescence Materials: Internal Mechanism, Design Strategy, and Potential Application. *Acc. Mater. Res.* **2021**, *2*, 644−654.
(35) Ma, X.-K.; Liu, Y. Supramolecular Purely Organic Room-Temperature Phosphorescence. *Acc. Chem. Res.* **2021**, *54*, 3403.
(36) Zhang, T.; Ma, X.; Wu, H.; Zhu, L.; Zhao, Y.; Tian, H. Molecular Engineering for Metal-Free Amorphous Materials with Room-Temperature Phosphorescence. *Angew. Chem., Int. Ed.* **2020**, *59*, 11206.
(37) Ma, X.; Wang, J.; Tian, H. Assembling-Induced Emission: An Efficient Approach for Amorphous Metal-Free Organic Emitting Materials with Room-Temperature Phosphorescence. *Acc. Chem. Res.* **2019**, *52*, 738−748.
(38) Sun, H.; Shen, S.; Zhu, L. Photo-stimuli-responsive Organic Room-Temperature Phosphorescent Materials. *ACS Mater. Lett.* **2022**, *4*, 1599−1615.
(39) Garain, S.; Wagalgave, S. M.; Kongasseri, A. A.; Garain, B. C.; Ansari, S. N.; Sardar, G.; Kabra, D.; Pati, S. K.; George, S. J. Anion−π-Induced Room Temperature Phosphorescence from Emissive Charge-Transfer States. *J. Am. Chem. Soc.* **2022**, *144*, 10854−10861.
(40) Li, D.; Yang, Y.; Yang, J.; Fang, M.; Tang, B. Z.; Li, Z. Completely aqueous processable stimulus responsive organic room temperature phosphorescence materials with tunable afterglow color. *Nat. Commun.* **2022**, *13*, 347.
(41) Wang, D.; Gong, J.; Xiong, Y.; Wu, H.; Zhao, Z.; Wang, D.; Tang, B. Z. Achieving Color-Tunable and Time-Dependent Organic Long Persistent Luminescence via Phosphorescence Energy Transfer for Advanced Anti-Counterfeiting. *Adv. Funct. Mater.* **2023**, *33*, No. 2208895.
(42) Lin, F.; Wang, H.; Cao, Y.; Yu, R.; Liang, G.; Huang, H.; Mu, Y.; Yang, Z.; Chi, Z. Stepwise Energy Transfer: Near-Infrared Persistent Luminescence from Doped Polymeric Systems. *Adv. Mater.* **2022**, *34*, No. 2108333.
(43) Dang, Q.; Jiang, Y.; Wang, J.; Wang, J.; Zhang, Q.; Zhang, M.; Luo, S.; Xie, Y.; Pu, K.; Li, Q.; Li, Z. Room-Temperature Phosphorescence Resonance Energy Transfer for Construction of Near-Infrared Afterglow Imaging Agents. *Adv. Mater.* **2020**, *32*, No. 2006752.
(44) Liang, Y. C.; Cao, Q.; Liu, K. K.; Peng, X. Y.; Sui, L. Z.; Wang, S. P.; Song, S. Y.; Wu, X. Y.; Zhao, W. B.; Deng, Y.; Lou, Q.; Dong, L.; Shan, C. X. Phosphorescent Carbon-Nanodots-Assisted Forster Resonant Energy Transfer for Achieving Red Afterglow in an Aqueous Solution. *ACS Nano* **2021**, *15*, 16242−16254.
(45) Huo, M.; Dai, X. Y.; Liu, Y. Ultrahigh Supramolecular Cascaded Room-Temperature Phosphorescence Capturing System. *Angew. Chem., Int. Ed.* **2021**, *60*, 27171−27177.
(46) Wang, X. F.; Xiao, H.; Chen, P. Z.; Yang, Q. Z.; Chen, B.; Tung, C. H.; Chen, Y. Z.; Wu, L. Z. Pure Organic Room Temperature Phosphorescence from Excited Dimers in Self-Assembled Nanoparticles under Visible and Near-Infrared Irradiation in Water. *J. Am. Chem. Soc.* **2019**, *141*, 5045−5050.
(47) Peng, H.; Xie, G.; Cao, Y.; Zhang, L.; Yan, X.; Zhang, X.; Miao, S.; Tao, Y.; Li, H.; Zheng, C.; et al. On-demand modulating afterglow color of water-soluble polymers through phosphorescence FRET for multicolor security printing. *Sci. Adv.* **2022**, *8*, No. eabk2925.
(48) Xu, W. W.; Chen, Y.; Lu, Y. L.; Qin, Y. X.; Zhang, H.; Xu, X.; Liu, Y. Tunable Second-Level Room-Temperature Phosphorescence of Solid Supramolecules Between Acrylamide-Phenylpyridium Copolymers and Cucurbit[7]uril. *Angew. Chem., Int. Ed.* **2022**, *61*, No. e202115265.
(49) Zhang, J.; Xu, S.; Zhang, L.; Wang, X.; Bian, Y.; Tang, S.; Zhang, R.; Tao, Y.; Huang, W.; Chen, R. Highly Efficient and Robust Full-Color Organic Afterglow through 2D Superlattices Embedment. *Adv. Mater.* **2022**, *34*, No. 2206712.
(50) Garain, S.; Garain, B. C.; Eswaramoorthy, M.; Pati, S. K.; George, S. J. Light-Harvesting Supramolecular Phosphors: Highly Efficient Room Temperature Phosphorescence in Solution and Hydrogels. *Angew. Chem., Int. Ed.* **2021**, *60*, 19720−19724.
(51) Zhang, Z.-J.; Zhang, Y.-M.; Liu, Y. Controlled Molecular Self-Assembly Behaviors between Cucurbituril and Bispyridinium Derivatives. *J. Org. Chem.* **2011**, *76*, 4682.
(52) Jeon, W. S.; Ziganshina, A. Y.; Lee, J. W.; Ko, Y. H.; Kang, J. K.; Lee, C.; Kim, K. A [2]pseudorotaxane-based molecular machine: reversible formation of a molecular loop driven by electrochemical and photochemical stimuli. *Angew. Chem., Int. Ed.* **2003**, *42*, 4097−4100.
(53) Ma, X. K.; Zhang, W.; Liu, Z.; Zhang, H.; Zhang, B.; Liu, Y. Supramolecular Pins with Ultralong Efficient Phosphorescence. *Adv. Mater.* **2021**, *33*, No. 2007476.
(54) Pazos, E.; Novo, P.; Peinador, C.; Kaifer, A. E.; Garcia, M. D. Cucurbit[8]uril (CB[8])-Based Supramolecular Switches. *Angew. Chem., Int. Ed.* **2019**, *58*, 403−416.
(55) Ko, Y. H.; Hwang, I.; Kim, H.; Kim, Y.; Kim, K. Molecular pop-up toy: a molecular machine based on folding/unfolding motion of alkyl chains bound to a host. *Chem. - Asian J.* **2015**, *10*, 154−159.
(56) Dai, X. Y.; Huo, M.; Dong, X.; Hu, Y. Y.; Liu, Y. Noncovalent Polymerization-Activated Ultrastrong Near-Infrared Room-Temperature Phosphorescence Energy Transfer Assembly in Aqueous Solution. *Adv. Mater.* **2022**, *34*, No. 2203534.

https://doi.org/10.1021/jacsau.3c00642
JACS Au XXXX, XXX, XXX−XXX

(57) Liu, Y.; Li, X.-Y.; Zhang, H.-Y.; Li, C.-J.; Ding, F. Cyclodextrin-Driven Movement of Cucurbit[7]uril. *J. Org. Chem.* **2007**, *72*, 3640.
(58) Pedrini, A.; Devi Das, A.; Pinalli, R.; Hickey, N.; Geremia, S.; Dalcanale, E. The Role of Chain Length in Cucurbit[8]uril Complexation of Methyl Alkyl Viologens. *Eur. J. Org. Chem.* **2021**, *2021*, 1547−1552.
(59) Liu, Z.; Liu, Y. Multicharged cyclodextrin supramolecular assemblies. *Chem. Soc. Rev.* **2022**, *51*, 4786−4827.
(60) Huo, M.; Dai, X. Y.; Liu, Y. Ultralarge Stokes Shift Phosphorescence Artificial Harvesting Supramolecular System with Near-Infrared Emission. *Adv. Sci.* **2022**, *9*, No. 2201523.
(61) Hu, Y. Y.; Dai, X. Y.; Dong, X.; Huo, M.; Liu, Y. Generation of Tunable Ultrastrong White-Light Emission by Activation of a Solid Supramolecule through Bromonaphthylpyridinium Polymerization. *Angew. Chem., Int. Ed.* **2022**, *61*, No. e202213097.
(62) Kirch, A.; Gmelch, M.; Reineke, S. Simultaneous Singlet-Singlet and Triplet-Singlet Forster Resonance Energy Transfer from a Single Donor Material. *J. Phys. Chem. Lett.* **2019**, *10*, 310−315.
(63) Kuila, S.; George, S. J. Phosphorescence Energy Transfer: Ambient Afterglow Fluorescence from Water-Processable and Purely Organic Dyes via Delayed Sensitization. *Angew. Chem., Int. Ed.* **2020**, *59*, 9393−9397.
(64) Knowles, K. E.; Malicki, M.; Weiss, E. A. Dual-Time Scale Photoinduced Electron Transfer from PbS Quantum Dots to a Molecular Acceptor. *J. Am. Chem. Soc.* **2012**, *134*, 12470−12473.
(65) Wang, S.; Li, H.; Huang, H.; Cao, X.; Chen, X.; Cao, D. Porous Organic Polymers as a Platform for Sensing Applications. *Chem. Soc. Rev.* **2022**, *51*, 2031−2080.

https://doi.org/10.1021/jacsau.3c00642
JACS Au XXXX, XXX, XXX−XXX